iPSC-Derived Macrophages Effectively Treat Pulmonary Alveolar Proteinosis in *Csf2rb*-Deficient Mice

Adele Mucci,[1,2,3] Elena Lopez-Rodriguez,[4,5] Miriam Hetzel,[1,2,3] Serena Liu,[6] Takuji Suzuki,[7,8] Christine Happle,[5,9] Mania Ackermann,[2,3,10] Henning Kempf,[3,11,16] Roman Hillje,[2,3,10] Jessica Kunkiel,[1,2,3] Ewa Janosz,[1,2,3] Sebastian Brennig,[2,3,10] Silke Glage,[3,12] Jens P. Bankstahl,[13] Sabine Dettmer,[14] Thomas Rodt,[14] Gudrun Gohring,[15] Bruce Trapnell,[7] Gesine Hansen,[5,9] Cole Trapnell,[6] Lars Knudsen,[4,5] Nico Lachmann,[2,3,10,17,*] and Thomas Moritz[1,2,3,17]

[1]Research Group Reprogramming and Gene Therapy, Hannover Medical School (MHH), Hannover, Germany
[2]Institute of Experimental Hematology, MHH, Hannover Medical School, Carl-Neuberg-Str.1, 30625 Hannover, Germany
[3]Cluster of Excellence REBIRTH, MHH, Hannover, Germany
[4]Department of Functional and Applied Anatomy, MHH, Hannover, Germany
[5]Biomedical Research in Endstage and Obstructive Lung Disease (BREATH), Member of the German Center for Lung Research (DZL), Hannover, Germany
[6]Department of Genome Sciences, Seattle, WA, USA
[7]Division of Pulmonary Biology, Perinatal Institute, Cincinnati Children's Hospital Medical Center, Cincinnati, OH, USA
[8]Division of Pulmonary Medicine, Jichi Medical University, Shimotsukeshi, Tochigi, Japan
[9]Department of Pediatric Pneumology, Allergology and Neonatology, MHH, Hannover, Germany
[10]Research Group Translational Hematology of Congenital Diseases, MHH, Hannover, Germany
[11]Leibniz Research Laboratories for Biotechnology and Artificial Organs (LEBAO), Department of Cardiac, Thoracic, Transplantation and Vascular Surgery, Hannover Medical School, Hannover, Germany
[12]Institute of Laboratory Animal Science and Central Animal Facility, MHH, Hannover, Germany
[13]Department of Nuclear Medicine, MHH, Hannover, Germany
[14]Department of Diagnostic and Interventional Radiology, MHH, Hannover, Germany
[15]Department of Human Genetic, MHH, Hannover, Germany
[16]Present address: Department of Stem Cell Biology, Novo Nordisk A/S, 2760 Maaloev, Denmark
[17]Co-senior author
*Correspondence: lachmann.nico@mh-hannover.de
https://doi.org/10.1016/j.stemcr.2018.07.006

SUMMARY

Induced pluripotent stem cell (iPSC)-derived hematopoietic cells represent a highly attractive source for cell and gene therapy. Given the longevity, plasticity, and self-renewal potential of distinct macrophage subpopulations, iPSC-derived macrophages (iPSC-Mφ) appear of particular interest in this context. We here evaluated the airway residence, plasticity, and therapeutic efficacy of iPSC-Mφ in a murine model of hereditary pulmonary alveolar proteinosis (herPAP). We demonstrate that single pulmonary macrophage transplantation (PMT) of $2.5–4 \times 10^6$ iPSC-Mφ yields efficient airway residence with conversion of iPSC-Mφ to an alveolar macrophage (AMφ) phenotype characterized by a distinct surface marker and gene expression profile within 2 months. Moreover, PMT significantly improves alveolar protein deposition and other critical herPAP disease parameters. Thus, our data indicate iPSC-Mφ as a source of functional macrophages displaying substantial plasticity and therapeutic potential that upon pulmonary transplantation will integrate into the lung microenvironment, adopt an AMφ phenotype and gene expression pattern, and profoundly ameliorate pulmonary disease phenotypes.

INTRODUCTION

Induced pluripotent stem cells (iPSCs), and thereof derived progeny, constitute a potentially unlimited, highly standardized source for cell and gene therapy (Takahashi and Yamanaka, 2006). With regard to diseases of the hematopoietic system, hematopoietic stem cells (HSCs) traditionally represent the prime target cells for transplantation and gene therapy approaches (Naldini, 2015); however, despite some recent success, the generation of transplantable HSCs from pluripotent cell sources remains problematic (Sugimura et al., 2017; Suzuki et al., 2013). On the other hand, transplantable and long-lived cells also exist in the myeloid compartment and here, in particular distinct tissue resident macrophage populations have been identified. Moreover, the generation of functional

macrophages from iPSCs (iPSC-Mφ) already has been established with considerable efficacy (Lachmann et al., 2015; Mucci et al., 2016; van Wilgenburg et al., 2013). The capacity of such iPSC-Mφ to long-term engraft in different organs and adopt an organ-specific tissue-resident macrophage (TRM)-like surface phenotype and gene expression pattern has been demonstrated (Happle et al., 2018; Litvack et al., 2016; Takata et al., 2017). Thus, iPSC-Mφ may serve as an innovative and highly standardized source for cell and gene therapy approaches.

Within the macrophage compartment, bone marrow-derived cells established from monocytes circulating in the blood stream have to be differentiated from TRM populations. The majority of TRM populations including microglia, Kupffer cells, Langerhans cells, and alveolar macrophages (AMφ) recently have been demonstrated to
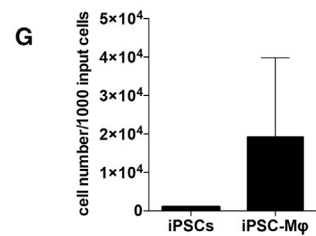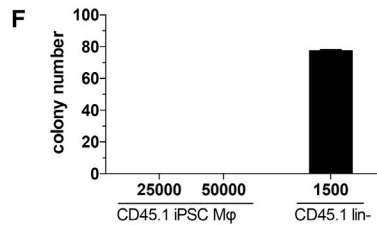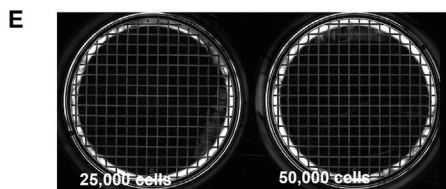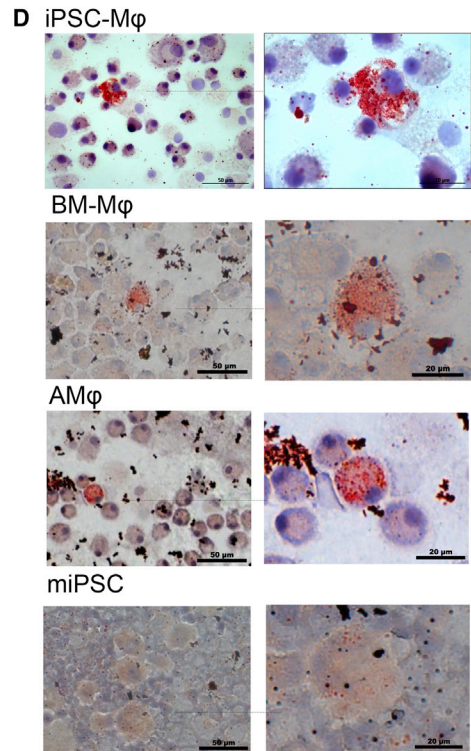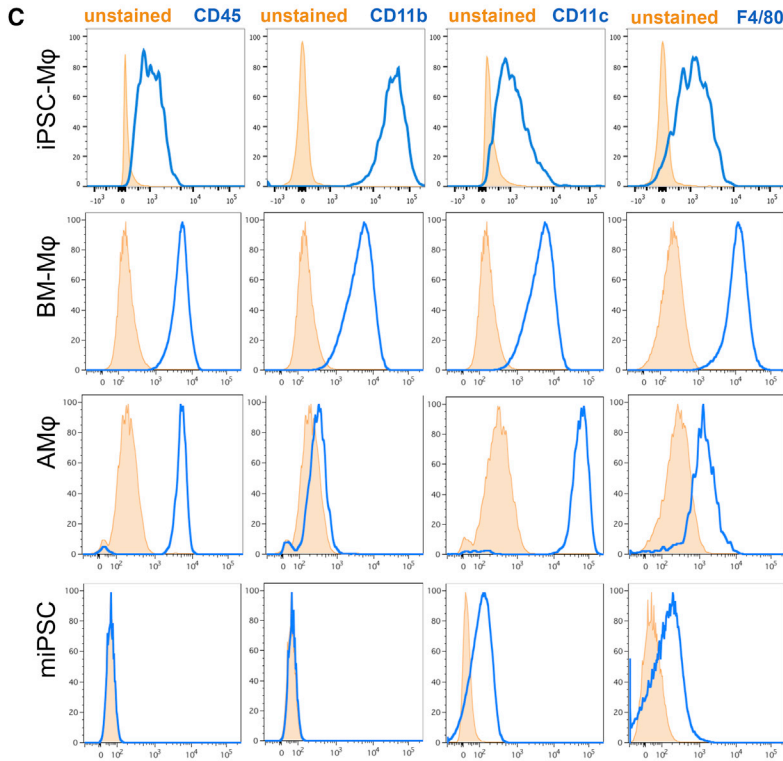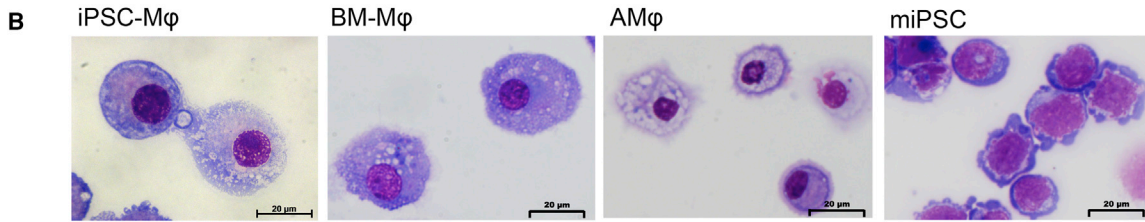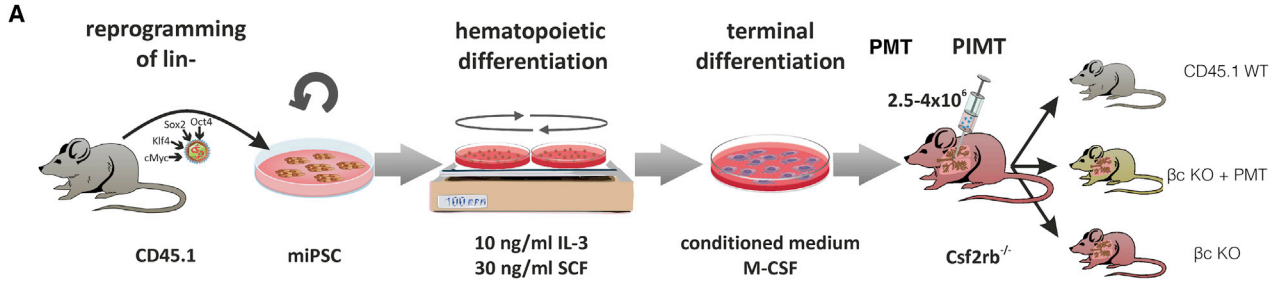
(legend on next page)

differentiate from an early precursor in the yolk-sac blood islands or the fetal liver, but independently from HSCs (Gomez Perdiguero et al., 2015; Guilliams et al., 2013; Hoeffel et al., 2015). Under physiological conditions these TRM populations sustain themselves throughout adult life, and only after the loss of the primary population due to disease or damage (e.g., radiation, infections) are significant amounts of TRMs replenished via peripheral blood monocytes (Bleriot et al., 2015; Lavin et al., 2014), similar to the process well established for cardiac or intestinal macrophages (Bain and Mowat, 2014; Epelman et al., 2014). In addition to their longevity and self-renewal properties, TRM populations are characterized by a substantial plasticity, as has been convincingly demonstrated by the transfer of distinct primary TRM populations into new tissue and organ microenvironments (Lavin et al., 2014).

Hereditary pulmonary alveolar proteinosis (herPAP) constitutes a rare life-threatening pulmonary disease caused by mutations in the granulocyte macrophage colony-stimulating factor (GM-CSF) receptor α or β chain genes (*CSF2RA* and *CSF2RB*, respectively) resulting in defective AMφ, and impaired capacity to clear the alveoli from surfactant factor and other lipoproteins, and subsequently severe respiratory insufficiency (Martinez-Moczygemba et al., 2008; Suzuki et al., 2011; Tanaka et al., 2011). Current treatment options are purely symptomatic and affected children rarely survive to adulthood, thus new therapeutic options are urgently required. To this point, two recent studies suggest that pulmonary macrophage transplantation (PMT) may constitute a suitable approach for cell-based gene therapy in herPAP patients (Happle et al., 2014; Suzuki et al., 2014a). Therefore, in the present study we evaluated a pulmonary transplantation scenario employing iPSC-Mφ in an established murine herPAP disease model based on *Csf2rb*-deficient mice (βc$^{-/-}$; βc knockout [KO]) (Nishinakamura et al., 1995). In addition to the therapeutic effect we carefully monitored the contribution of progeny derived from transplanted iPSC-Mφ to bronchoalveolar as well as pulmonary cellularity and performed extensive gene expression analysis in iPSC-Mφ progeny recovered 2 months following PMT.

RESULTS

Generation and Characterization of iPSC-Mφ

To allow for the convenient *in vivo* tracking of iPSC-Mφ in the CD45.2$^+$ βc KO recipients, iPSC-Mφ were generated from a congenic CD45.1$^+$ iPSC line. An embryoid body-based differentiation procedure (Mucci et al., 2016; Pfaff et al., 2012), followed by terminal differentiation with M-CSF, was employed to yield cells displaying macrophage-typical morphology, surface marker expression (CD45, CD11b, CD11c, and F4/80), as well as the capacity to take up surfactant material from murine bronchoalveolar lavage fluid (BALF) following GM-CSF stimulation (Figures 1A–1D). iPSC-Mφ failed to form colonies in clonogenic assays, thus excluding a significant contribution of hematopoietic progenitors (Figures 1E and 1F). Furthermore, the overall differentiation process from iPSC to iPSC-Mφ was associated with an approximately 2-fold cell expansion (Figure 1G), thereby facilitating the production of relevant quantities of iPSC-Mφ for transplantation scenarios.

Airway Residence of iPSC-Mφ in βc$^{-/-}$ Mice

Next, we performed transplantation experiments by intra-tracheal administration of 2.5–4 × 10^6 iPSC-Mφ into the lungs of βc$^{-/-}$ recipient mice. Two months later, airway residence was evaluated in the lungs and BALF of the animals. At this time point a distinct population of CD45.1$^+$ cells was detectable in the lungs and BALF of recipients with the efficacies of airway residence ranging from 0.2% to 6% (1.3 ± 1.9, mean ± SD) CD45.1$^+$ cells in the lungs and 0.2% to 15% (2.7 ± 4.7, mean ± SD) in the BALF (Figures 2A and 2B). As evident from flow cytometry and immunofluorescence staining of pulmonary tissue sections, donor-derived cells localized predominantly within the alveolar spaces (Figure 2C), and upon retrieval and characterization of these CD45.1$^+$ cells from the lungs and BALF, cells displayed typical macrophage morphology on cytospins (Figures 2D and S1A), confirming the persistence of donor-derived macrophages following PMT. CD45.1$^+$ cells also revealed co-expression of the alveolar macrophage surface marker

Figure 1. Characterization of iPSC-Mφ

(A) Schematic description of study design: generation of iPSCs was followed by differentiation in and embryoid body-based protocol into macrophages, which are then transplanted in the lungs (PMT) of β KO mice.

(B) Typical Mφ morphology of iPSC-Mφ, BM-Mφ, AMφ in contrast to undifferentiated iPSC in May-Gruenwald/GIEMSA-stained cytospins. Scale bars, 20 μm.

(C) Surface markers expression of iPSC-Mφ, BM-Mφ, AMφ, and miPSC by flow cytometry (CD45, CD11b, CD11c, and F4/80, orange-filled line unstained and blue line for marker expression).

(D) Representative picture of surfactant uptake visualized by oil red O staining. Scale bars, 50 and 20 μm.

(E and F) Clonogenic potential of iPSC-Mφ seeded (25,000 and 50,000 per mL) (E) and quantification of colony numbers compared with BM control cells (F) (technical replicates n = 2; mean ± SD).

(G) Differentiation efficiency of iPSCs into Mφ (independent experiments n = 3, mean ± SD).
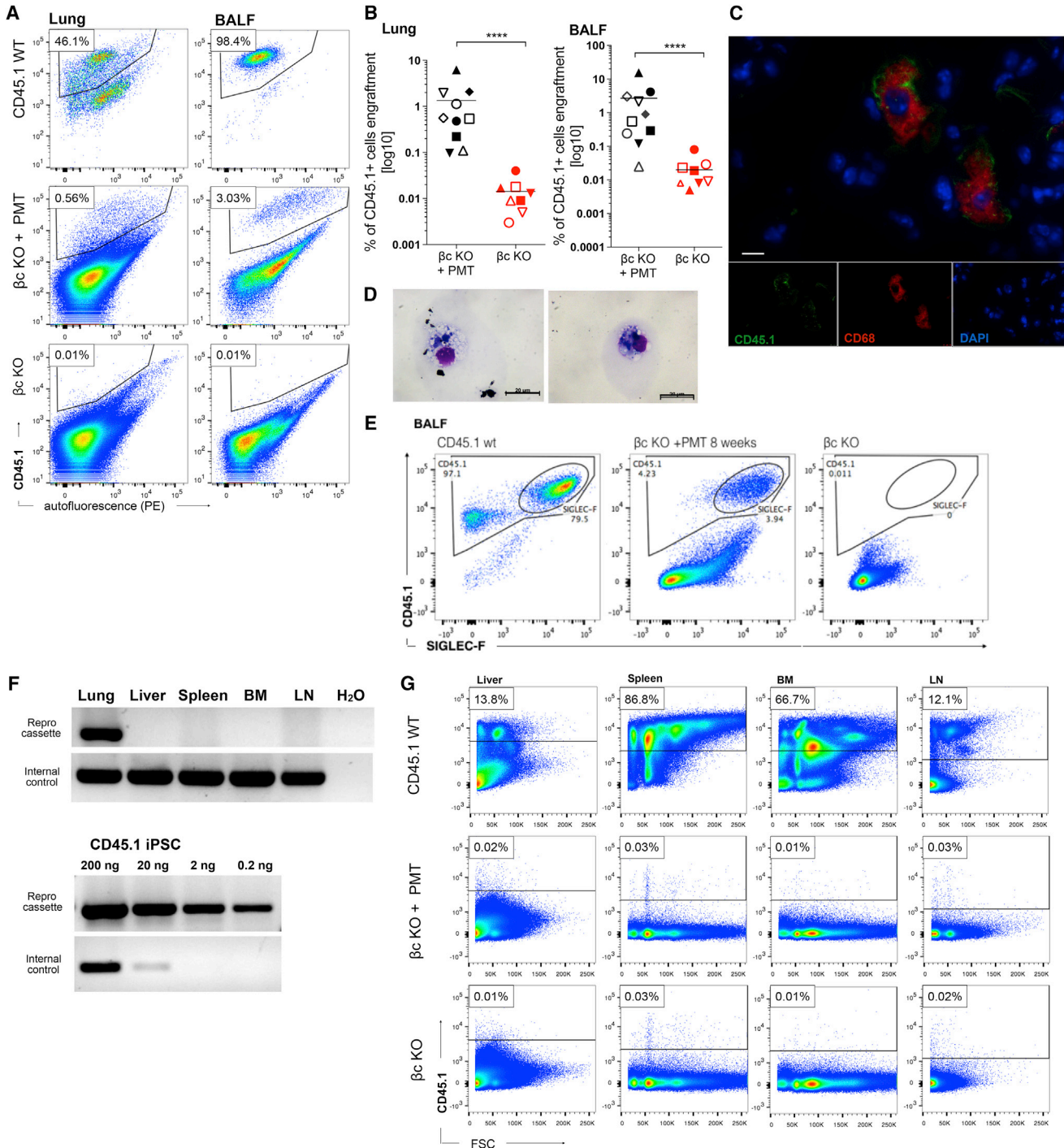
Figure 2. iPSC-Mφ Engraftment in βc KO Mice upon PMT

(A) CD45.1^{+} cells in the lungs and BALF of recipient mice (βc KO + PMT) and CD45.1 WT and βc KO controls.

(B) Corresponding percentage values for of all transplanted animals (independent experiments n = 6; 10 βc KO + PMT mice, 8 βc KO mice; means) 2 months post transplantation.

(C) Localization and phenotype of recovered cells staining positive for CD45.1 (green), CD68 (red), and DAPI (blue) (immunofluorescence analysis of cryopreserved lung section). Scale bar, 10 μm.

(D) Macrophage morphology of recovered CD45.1^{+} cells (May-Gruenwald/GIEMSA-stained cytospins). Scale bar, 20 μm. Two months post transplantation.

(legend continued on next page)

Table 1. Airway Residence and Alveolar Protein Concentration in Transplanted Mice 6 Months after Pulmonary Transplantation of iPSC-Mφ

Transplanted Cell Number	Engraftment in Lung (%)	Engraftment in BALF (%)	BALF Protein Concentration (μg/mL)
4×10^6	0.002	0.009	920
4×10^6	1.3	7.84	573
4×10^6	0.63	0.52	927
4.8×10^6	2.05	4.96	575
No cells	0.011	0.006	727.089

BALF, bronchoalveolar lavage fluid.

SIGLEC-F in flow cytometry at comparable levels to wild-type (WT) cells (Figure 2E). Airway residence of CD45.1$^+$ cells also was observed in the BALF (0.6%–7.8%) and lungs (0.5%–2.0%) of three out of four mice analyzed 6 months after single transplantation of 4–4.8 × 10^6 cells, with two of these mice demonstrating quite high levels of airway residence (Table 1).

No iPSC-derived cells were detected in the bone marrow, liver, lymph nodes, or spleen of recipient animals even when sensitive, PCR-based methodology (detection limit <10^{-3}) was employed, indicating the high organ-specificity of iPSC-Mφ engraftment (Figures 2F and 2G). This highly efficient, organ-specific engraftment most likely is caused by the profoundly elevated pulmonary GM-CSF levels present in βc$^{-/-}$ mice as well as PAP patients, which serve as part of a feedback loop aiming at the correction of the deficiency of AMφ in herPAP (Suzuki et al., 2014a).

Influence of the Lung Microenvironment on the Transcriptional Profile of Transplanted iPSC-Mφ

To stringently characterize our iPSC-Mφ population before and after pulmonary transplantation on a molecular level, gene expression profiling was performed on (1) pre-transplantation iPSC-Mφ, (2) Mφ obtained by *in vitro* differentiation of murine lineage-negative bone marrow cells (BM-Mφ), (3) non-differentiated CD45.1 iPSC, (4) murine alveolar Mφ (AMφ) isolated from the BALF of healthy control mice, and (5) iPSC-Mφ recovered from the transplanted animals 2 months after (PMT-Mφ). For populations (4) and (5) purities of 77.6% SIGLEC-F$^+$ and 88.4% CD45.1$^+$ cells, respectively, were documented by flow cytometric analysis after sorting (Figures S2A and S2B).

Whole transcriptome analysis revealed our iPSC-Mφ to closely resemble BM-Mφ (Figure 3) despite the *Myb*-independent, "embryonic type" nature of iPSC-Mφ documented in the current literature (Buchrieser et al., 2017; Litvack et al., 2016; Takata et al., 2017). Thus, we regard the transcriptional closeness between the iPSC-Mφ and the BM-Mφ population primary as an *in vitro* cell culture artifact reflecting the similar culture conditions under which these two populations were generated. To gain further insights into the ontogeny and transcriptional fingerprint of our murine iPSC-Mφ, we added a side-by-side analysis of iPSC-Mφ and BM-Mφ only, and performed gene set enrichment analysis utilizing previously published gene sets for primitive, yolk-sac-derived, or adult-type, bone marrow-derived macrophages (Figures S3A and S3B) (Takata et al., 2017). This analysis clearly demonstrates that our iPSC-derived macrophages share more genes with yolk-sac-derived macrophages (left panel) than BM-Mφ (right panel).

Furthermore, iPSC-Mφ did not retain remnants of the iPSC gene expression pattern and shared few similarities with AMφ. Gene set enrichment analysis using the mSigDB's chemical and genetic perturbations collection confirmed that iPSCs expressed embryonic stem cell genes that were downregulated in iPSC-Mφ. Upon transplantation, iPSC-Mφ acquired more similarities to AMφ in their transcriptional signature, while losing similarities to their *in vitro* counterpart. Indeed, PMT-Mφ had 1,152 differentially expressed genes compared with AMφ, while 2,332 genes changed expression levels from iPSC-Mφ. Based on the differential gene expression between the five populations, six clusters were determined and aligned to enriched gene sets according to the gene ontology (GO) gene set collection (Table S1).

Cluster 1 was selectively expressed in undifferentiated iPSCs, in such a cluster several pathways are involved in cell cycle and cell proliferation and even in telomere and DNA damage mechanisms, in line with the stemness of these cells. AMφ revealed upregulation of genes of cluster 2 involved in several pathways of circadian clock. BM-Mφ and iPSC-Mφ shared expression of cluster 3 that are involved in several immune pathways. Both AMφ and PMT-Mφ downregulated genes of cluster 5, while only PMT-Mφ revealed increased expression of cluster 4. However, no gene set was significantly enriched in cluster 4.

Analysis of selected gene sets associated with Mφ, AMφ, pluripotency, or self-renewal further confirmed the distinct expression patterns of the investigated cell populations, as

(E) Co-expression of CD45.1 and SIGLEC-F on BALF cells measured by flow cytometry.
(F) Selective lung but no other organs engraftment assessed by genomic DNA PCR (independent experiments n = 3, 5 transplanted mice).
(G) flow cytometry (representative flow charts shown for CD45.1. WT, βc KO + PMT 2 months post transplantation and non-transplanted βc KO animals).
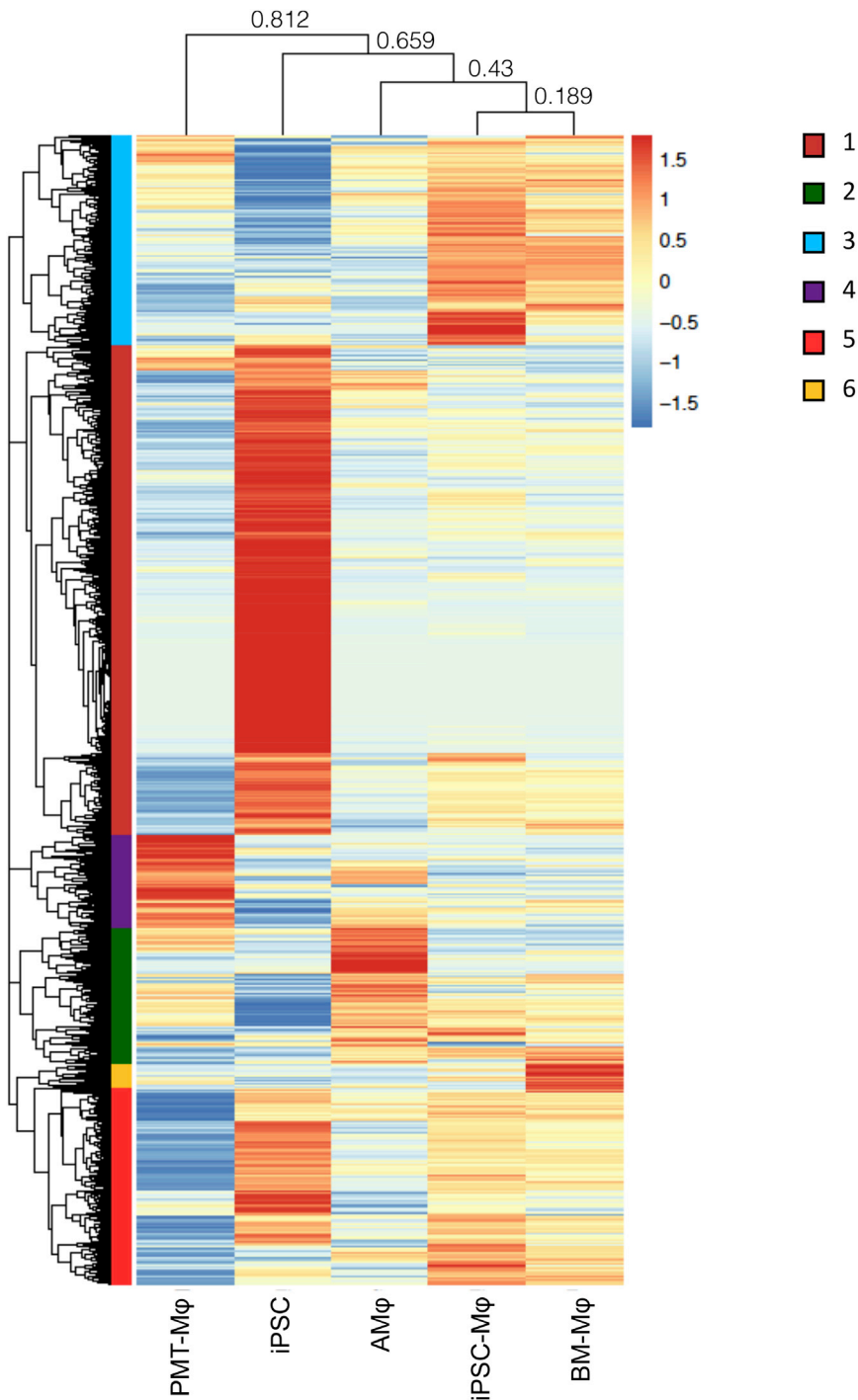****p < 0.0001 in Mann-Whitney test; BM, bone marrow; LN, lymph nodes.

Figure 3. Heatmap Comparing Transcriptional Profiles

According to the RNA sequencing results, the heatmap shows the expression profiles of iPSCs, iPSC-derived macrophages prior to transplantation (iPSC-Mφ), bone marrow-derived macrophages (BM-Mφ), alveolar macrophages isolated from WT animals (AMφ), and iPSC-Mφ recovered from the lungs of transplanted βc KO animals (PMT-Mφ). Six clusters were identified depending on the populations expression profiles (independent experiments n = 2).

well as the alveolar phenotype acquired upon transplantation of iPSC-Mφ. Whereas all macrophage populations expressed genes classically associated with this cell type, such as *Csf1*, *2*, and *3* receptors, *Emr1* or *Mrc1* (Figure 4A), AMφ but also PMT-Mφ recovered from the animals showed a more specific AM-type gene expression including *Pparγ*, *Cd74*, and *Siglec5* (Figure 4B). Pluripotency, as well

as self-renewal-associated genes were primarily expressed in iPSCs, although some genes that were recently described in the context of TRM self-renewal, such as *Myc* and *Klf-4* (Soucie et al., 2016), were expressed, particularly in AMφ (Figures 4C and 4D). Of note, PMT-Mφ also upregulated genes associated with self-renewal upon their residence in the specific microenvironment. This indicates how much
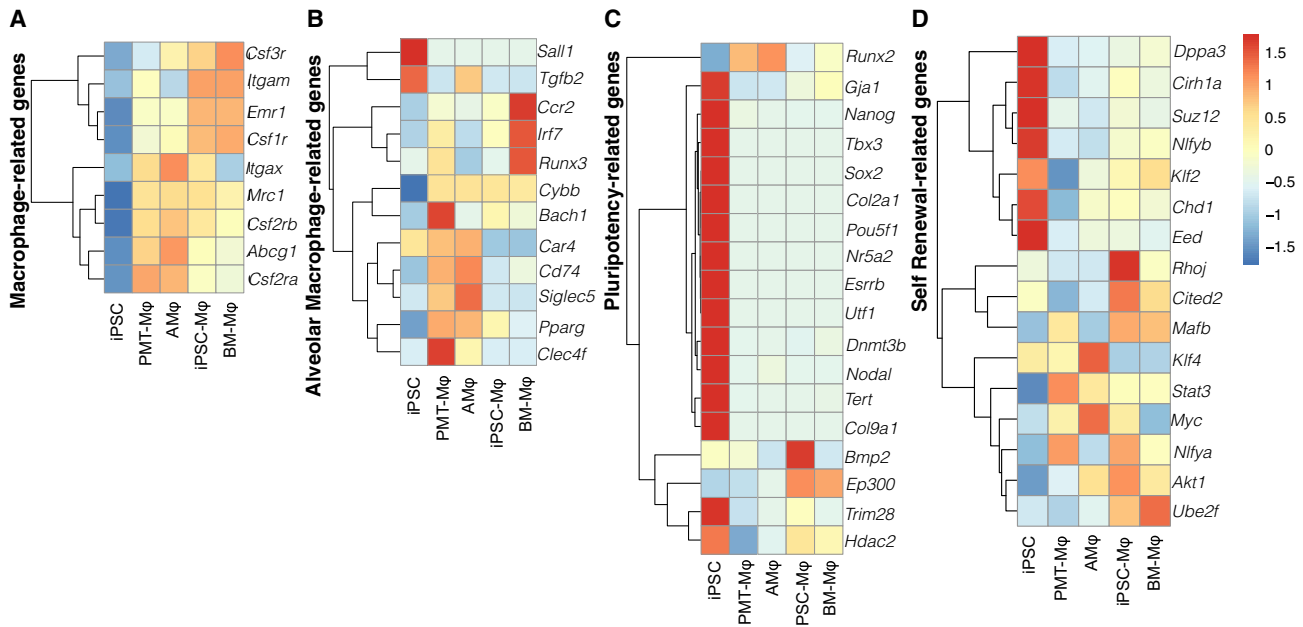
Figure 4. Heatmaps of Selected Genes Involved in Macrophages, Alveolar Macrophages, Pluripotency, and Self-Renewal
Expression in iPSC, iPSC-Mφ, BM-Mφ, and PMT-Mφ of selected genes characteristic of (A) macrophage functions, (B) alveolar macrophages, (C) involved in pluripotency, and (D) in self-renewal (independent experiments n = 2).

these cells can adapt to not only the specific functionality of alveolar macrophages, but also their transcriptional signature.

Principal component analysis of the different samples revealed selective clustering of populations (Figure 5A), and, in particular, undifferentiated iPSCs were clearly separated from the differentiated cell types. As expected, iPSC-Mφ before transplantation clustered closely with BM-Mφ, while after transplantation PMT-Mφ acquired more similarities with AMφ, suggesting tissue-specific adaptation of these cells upon contact with the specific microenvironment. When compared with iPSCs, evaluation of differentially regulated genes within the macrophage populations revealed major similarities between BM-Mφ, iPSC-Mφ, and PMT-Mφ, with 935 upregulated genes shared in all populations (Figure 5B). These 935 upregulated genes are mostly involved in biological processes of inflammatory and immune response (Figure 5C, left). In addition, PMT-Mφ shared 299 upregulated genes with AMφ, with major involvement in immune processes and antigen presentation (Figure 5C, right). A similar picture was obtained when downregulated genes were analyzed, with 974 genes similarly regulated between the three macrophage populations (Figure 5D). These genes that are downregulated upon differentiation from iPSC are involved in cell cycle, cell division, as well as DNA replication pathways (Figure 5E). Finally, specific analysis evaluating the changes of gene expression upon differentiation from iPSC to

iPSC-Mφ, and upon transplantation toward AMφ, identified 18 (Omics explorer) or 19 (Perseus) genes that change in expression during this process (Figure 5F). Clustering of these genes confirms the close proximity of iPSC-Mφ to BM-Mφ and of PMT-Mφ to AMφ (Figure 5G).

Therapeutic Efficacy of iPSC-Mφ

Next, we analyzed the therapeutic effects of iPSC-Mφ-based PMT in our *Csf2rb*-deficiency mouse model, i.e., the ability to clear alveolar surfactant material and to improve critical disease parameters. As a first evidence of therapeutic efficacy we observed markedly reduced opacity and a significant reduction of protein levels in the BALF 2 months after transplantation when compared with non-treated controls (Figures 6A and 6B). Profound improvements also were observed in other parameters such as BALF levels of GM-CSF, M-CSF, and surfactant protein D (Figures 6C–6E). Moreover, computed tomography (CT) scans revealed considerable improvements in lung densities in transplanted animals (Figures 6F and 6G) and, upon quantitative histology of lung sections, a significant reduction of intra-alveolar PAS-positive material was observed (Figures 6H and 6I).

Marked reduction in BALF and pulmonary protein levels also was observed at 6 months after transplantation in those two mice, with a high contribution of transplanted cells to BALF and lung cellularity (Table 1). These data highlight the capacity of the transplanted healthy cells to clear
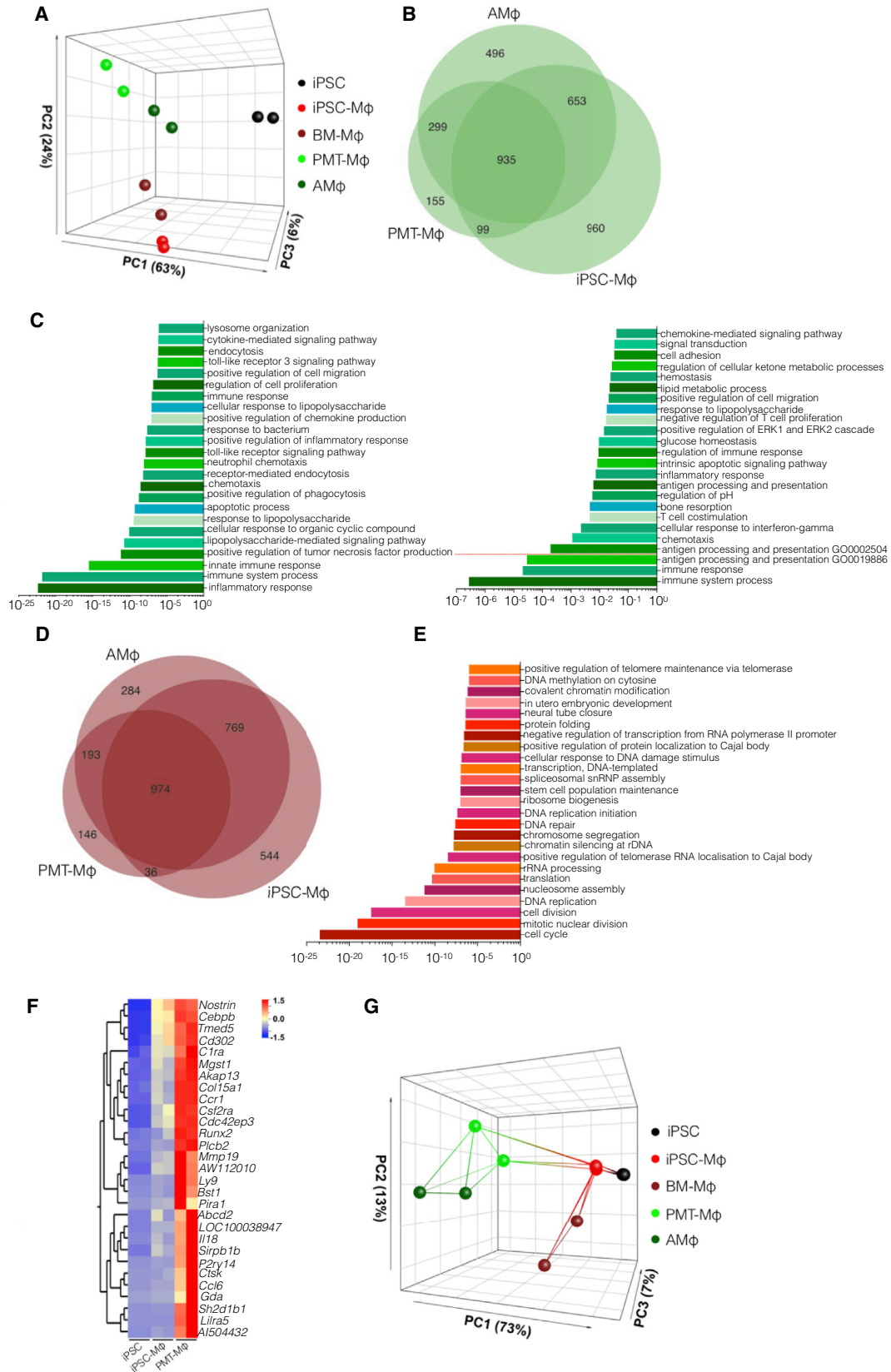
(legend on next page)

the deposited alveolar surfactant material and ameliorate the disease phenotype in βc KO mice. iPSC-Mφ transplantation was well tolerated and no evidence of procedure-related pathology such as teratoma formation was detected in the lungs or other organs (Figure S1B). Furthermore, histological analysis of various organs and tissues (liver, spleen, sternum, kidney, brain, fat, muscle, and heart) of transplanted animals revealed no signs of inflammation or fibrotic reactions (Figure S1C), further endorsing the clinical feasibility of our iPSC-Mφ-based PMT approach.

DISCUSSION

We here efficiently generated functional murine Mφ from an iPSC source, which, upon intra-tracheal transplantation, were able to engraft in the recipients' lungs, adapt to the pulmonary microenvironment, and improve critical disease parameters in a well-established murine herPAP disease model. Single applications of 2.5–4 × 10^6 iPSC-Mφ yielded engraftment for up to 6 months exclusively to the lung microenvironment, with rapid conversion of transplanted iPSC-Mφ to an AMφ-like phenotype characterized by the surface markers CD45.1, SIGLEC-F, and CD68 (macrosialin), classical macrophage morphology, and a distinct gene expression profile. Moreover, profound amelioration of the disease phenotype was observed in mice analyzed at the 2-month time point, and alveolar protein content also was improved in two of four mice analyzed after 6 months.

Of note, in our hands, profound improvements in her-PAP symptoms were obtained, although the transplanted iPSC-Mφ population showed considerable differences to AMφ by gene expression analysis, whereas cells recovered at the 2-month time point closely resembled AMφ. These data demonstrate the substantial plasticity of iPSC-Mφ resembling the properties previously described for other Mφ populations and, over time, allowing them to adopt classical functions of AMφ, such as surfactant clearance from the alveoli (Hussell and Bell, 2014). Importantly, despite the close molecular relationship of our iPSC-Mφ to the BM-Mφ population, we consider our IPSC-derived macrophages as a *Myb*-independent, embryonic-type population in accordance with the current literature on this topic (Buchrieser et al., 2017; Litvack et al., 2016; Takata et al., 2017), whereas we regard the molecular similarity between iPSC-Mφ and BM-Mφ, as displayed in the non-hierarchical clustering analysis, primarily as an *in vitro* cell culture artifact reflecting the similar culture conditions (including long-term M-CSF exposure) employed to generate these two populations. The *Myb*-independent, embryonic ontogeny of our iPSC-Mφ was supported by side-to-side gene set enrichment analysis of iPSC-Mφ and BM-Mφ. This consistency of our data argues for homolog cell populations used for array analysis despite a purity of only 78%–88% displayed by flow cytometry.

With respect to the therapeutic effect, it bears considerable interest that progressive improvement of PAP symptoms for more than a year, and prolonged survival, have been described following the PMT of BM-Mφ (Suzuki et al., 2014a). Given the profound overlap in phenotype, gene signature, and functionality between iPSC-Mφ and BM-Mφ, we anticipate similar long-term therapeutic efficacy also for PMT strategies employing iPSC-Mφ. Moreover, local or systemic administration of iPSC-Mφ also might represent a new approach to other macrophage- or TRM-related congenital diseases such as heme oxygenase-1 deficiency (Kovtunovych et al., 2014), adrenoleukodystrophy (Biffi et al., 2011; Cartier et al., 2014), autosomal recessive osteopetrosis (Neri et al., 2015), Gaucher disease (Sgambato et al., 2015), mucopolysaccharidosis type I (Viana et al., 2016), or severe combined immunodeficiency secondary to adenosine deaminase deficiency (Litvack et al., 2016). Clinical translation of iPSC-Mφ-based treatment approaches in these diseases most likely will involve the transplantation of genetically corrected, autologous iPSC-Mφ populations. In this regard, gene correction of PAP patient-derived iPSCs already has been demonstrated to reverse, at least *in vitro*, not only the PAP phenotype but also the associated functional defects (Lachmann et al., 2014; Suzuki et al., 2014b). While this work employed a lentiviral vector-based gene addition approach, modern designer nucleases even allow for the site-specific correction of defective genes, thus preserving physiologic gene regulation and avoiding the risk of insertional mutagenesis (Xu et al., 2015). In this context, a major advantage of iPSC-Mφ over BM-Mφ constitutes their almost unlimited potential for

Figure 5. RNA-Seq-Based Comparison of Cells Recovered from PMT 2 Months Post Transplantation
(A–C) (A) Principal-component analysis (PCA) of RNA-seq data, (B) Venn diagram of upregulated genes overlap between iPSC-Mφ, AMφ, and PMT-Mφ compared with iPSC, and (C) the gene ontology analysis for biological processes for the 935 genes concomitantly upregulated in all the three populations (left, significance ≤5% false discovery rate [FDR]) and for the 299 genes upregulated in both PMT-Mφ and AMφ (right, red line indicates a significance ≤5% FDR).
(D and E) Venn diagram of downregulated genes between the three cell types compared with iPSC (D) and corresponding gene ontology analysis of the shared 974 genes (E).
(F) Heatmap of genes successively upregulated during differentiation from iPSC to Mφ and after transplantation.
(G) PCA clustering of the identified genes represented in the heatmap (independent experiments n = 2).
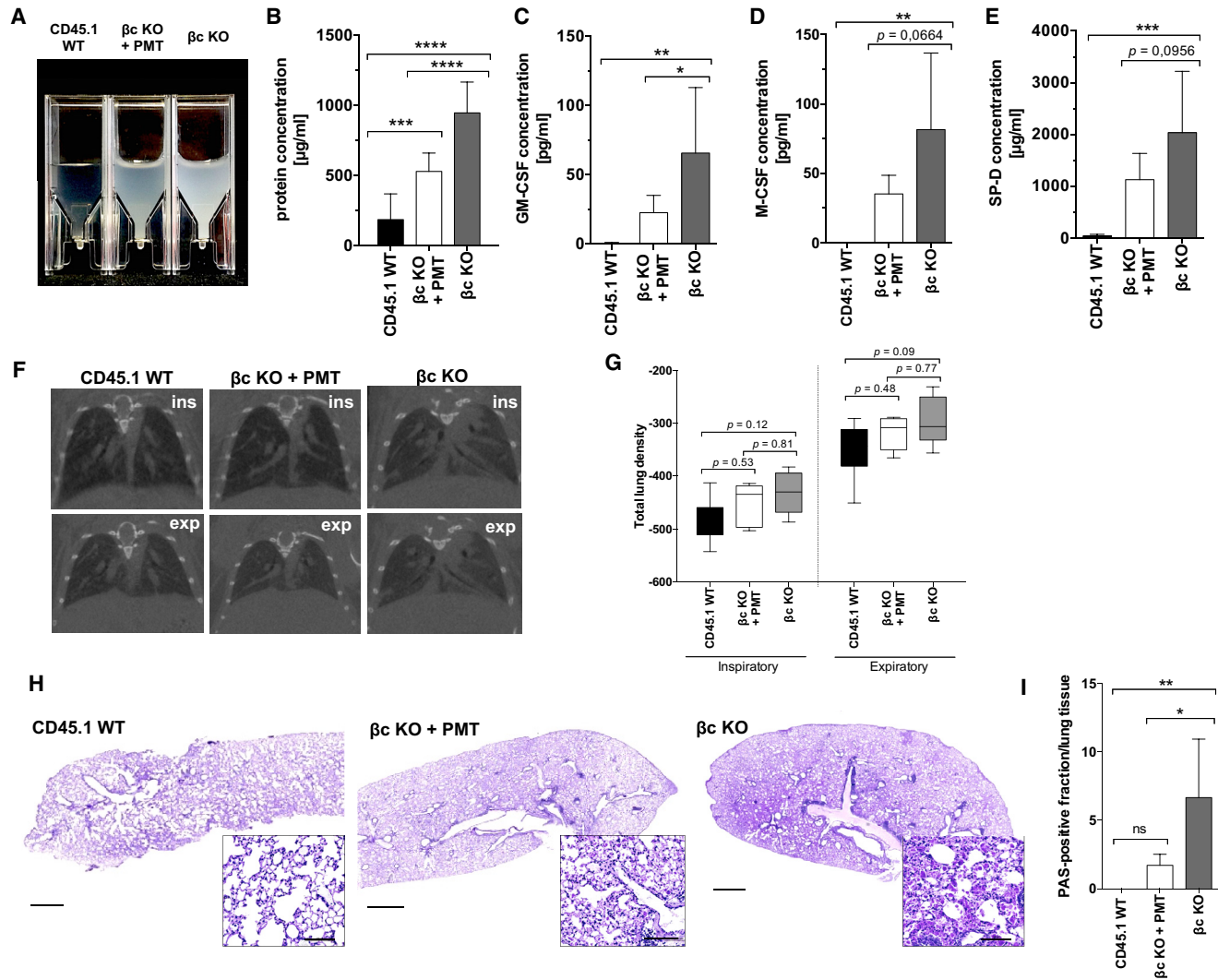
Figure 6. Therapeutic Efficacy of iPSC-Mφ-Based PMT

(A) Opacity of BALF from CD45.1 WT, βc KO + PMT, and βc KO mice.

(B) Total protein concentration in BALF (independent experiments n = 6; 10 βc KO + PMT mice, 9 CD45.1 WT mice, and 8 βc KO control mice; mean ± SD).

(C–E) GM-CSF (C), M-CSF (D), and SP-D (E) levels in BALF (independent experiments n = 3; 6 mice per group; mean ± SD).

(F and G) Representative pictures of CT scan (F) and quantification of lung density during inspiratory and expiratory phase (G) (independent experiments n = 3; 5 mice per group; mean ± SD).

(H and I) Lung histology after staining with PAS (H) (scale bars, 1 mm and 100 μm) and quantification of PAS-stained surfactant material (I) (independent experiments n = 3, 5 mice per group; mean ± SD; *p < 0.05, **p < 0.01, ***p < 0.001, ****p < 0.0001, respectively, in one-way ANOVA test; ns, not significant).

genetic modification at the pluripotent level. If exploited in a modular fashion this would allow for the generation of macrophages displaying multiple new efficacy and safety features upon differentiation. In addition, iPSCs can in principal be expanded indefinitely *ex vivo*, and we and others recently have developed *in vitro* differentiation protocols, which, at least in the human system, allow to continuously generate large quantities of macrophages of defined quality

as an important first step toward clinical application of these cells (Buchrieser et al., 2017; Lachmann et al., 2015). Clinical application of iPSC-Mφ also should benefit from the fact that organotropic transplantation, in contrast to allogeneic bone marrow transplantation or HSC-based gene therapy approaches, can be performed without prior chemo- and/or radiotherapeutic conditioning of the recipient. Although successful HSC-based gene therapy has been

demonstrated in βc KO mice (Kleff et al., 2008), in the clinical setting the severely damaged lungs of PAP patients represent a considerable risk factor during the conditioning procedure (Martinez-Moczygemba et al., 2008).

In summary, we here introduce iPSC-Mφ as an innovative, well-characterized, and abundant cell source, with long-term engraftment capacity and significant clinical efficacy in macrophage-related diseases such as herPAP, thus reiterating the profound clinical potential of iPSC-based treatment strategies.

EXPERIMENTAL PROCEDURES

Mice
B6.SJL-Ptprc[a]-Pep3[b]/BoyJ (CD45.1 WT) control mice were obtained from the central animal facility of Hannover Medical School. Csf2rb$^{-/-}$ BL/6 mice (βc KO) were obtained from The Jackson Laboratory and held in the central animal facility of Hannover Medical School. The Lower Saxony State animal welfare committee approved all animal experiments.

Differentiation of Murine iPSCs into Macrophages
CD45.1 iPSCs were maintained in pluripotent state as described previously (Ackermann et al., 2014). Differentiation was performed after passaging the cells for 2 days in feeder-free conditions on a gelatin-treated plate in an IMDM medium (Thermo Fisher Scientific) containing 10% fetal calf serum (FCS; Millipore), 1 mM penicillin-streptomycin, 150 μM monothioglycerol, and 10^3 U/mL leukemia inhibitory factor (pre-culture medium). For embryoid body formation, single cells were seeded at a density of 10,000 cells/mL in differentiation medium I: IMDM medium with 15% pre-tested FCS (ES-Cult FBS, STEMCELL Technologies), 1 mM penicillin-streptomycin, 1 mM L-glutamine, 50 ng/mL ascorbic acid (Sigma-Aldrich), and 150 mM monothioglycerol (Sigma-Aldrich). After 5 days, the medium was supplemented with 10 ng/mL murine interleukin-3 and 30 ng/mL murine stem cell factor (PeproTech) (Mucci et al., 2016; Pfaff et al., 2012). After 7 days, the embryoid bodies were dissociated into single cells using collagenase IV (250 U/mL, Life Technologies) and transferred into a suspension-culture plate with differentiation medium II: RPMI medium (Thermo Fisher Scientific) supplemented with 10% FCS, 1 mM L-glutamine, 1 mM penicillin-streptomycin, and 30% supernatant of L929 producer cells (Ladner et al., 1988) as a source of M-CSF.

Oil Red O Staining
iPSC-Mφ were pre-stimulated for 5 days with GM-CSF, and subsequently 200 μL of BALF (1:5 dilution) from herPAP mice was added to the medium. Twenty-four hours later, cells were collected, spun down, and stained with oil red O (Sigma-Aldrich). In brief, oil red O powder was solved in 99% 2-propanol (Roth). Fresh working solution was prepared by diluting 3 parts of oil red O in 2 parts of water. Cells were fixed in 10% formaldehyde (AppliChem) for 30 min and then treated with 60% 2-propanol for 5 min. Oil red O staining was performed for 10 min, and then the cells were washed and counterstained with hematoxylin.

RNA Sequencing
To isolate in-vivo-derived alveolar Mφ, C57BL/6 CD45.1 mice were sacrificed and bronchoalveolar lavage was performed to isolate SIGLEC-F^{+} cells via fluorescence-activated cell sorting (FACS). PMT-Mφ were recovered from transplanted animals based on CD45.1 expression by FACS from BALF and lungs. In addition, iPSCs, BM-, and iPSC-Mφ from in vitro differentiation were harvested by trypsinization. For all cells, RNA was isolated using the RNAeasy Plus Micro Kit (QIAGEN). Total RNA (10 ng) was amplified using the Ovation RNA-Seq System v.2 (NuGEN) according to the manufacturer's protocol. The libraries were prepared with the Nextera XT DNA Sample Preparation Kit (Illumina) and the concentrations were measured using the Qubit dsDNA HS (High Sensitivity) assay. The size of the libraries for each sample was measured using the Agilent HS DNA chip. The libraries were sequenced on an Illumina HiSeq 2500 in Rapid Mode, generating 20 million or more high-quality 75-base-paired long end reads per sample in the Gene Expression Core Facility and DNA Sequencing Core in Cincinnati Children's Hospital Medical Center.

RNA Sequencing Analysis
Sequence data were analyzed using the Cufflinks suite v.2.2.1 (Trapnell et al., 2012). Reads were mapped to the mouse reference genome (mm10) using TopHat v.2.0.13 (mouse gene annotations from GENCODE v.M2), with Bowtie v.2.2.3, quantified using Cuffquant, then analyzed for differential expression using Cuffdiff. Heatmaps of gene expression across the four conditions were generated using the R package pheatmap (Kolde, 2015); genes were clustered based on the Jensen-Shannon divergence metric described previously by Trapnell et al. (2010, 2012), and all heatmaps were row-scaled. Genes differentially expressed between iPSCs and iPSC-Mφ (q ≤ 0.05) were identified, and gene set enrichment analysis was performed with the piano R package (Varemo et al., 2013) using MsigDB's chemical and genetic perturbation gene set collection, and using mean as the statistical gene set analysis method. The piano package was also used to identify GO terms enriched in the annotated heatmap gene clusters (q ≤ 0.1) using a one-tailed Fisher's exact test. Principal component analysis (PCA) was conducted using Omics Explorer (Qlucore v.3.1). PCA data were visualized with RStudio (v.3.3.1) and the scatterplot3d package (v.0.3-40). To identify genes that are successively upregulated over time during transition from iPSC stage to iPSC-Mφ, and further following PMT-iPSC, two different strategies were applied: (1) two group comparisons for iPSC < iPSC-Mφ and iPSC-Mφ < PMT-Mφ (p < 0.05) were performed using Omics Explorer and (2) the profile plot tool in Perseus (Tyanova et al., 2016) was applied (reference profile: iPSC = −5, iPSC-Mφ = 0, PMT-Mφ = 5). Cell sorting purity is shown in Figures S3A and S3B. The identified sets of genes were visualized in a heatmap using Omics Explorer and a PCA, including the respective data from isolated BM-Mφ and AMφ. The processed RNA sequencing dataset was deposited in the Array Express database under accession number Array Express: E-MTAB-6442.

Pulmonary Transplantation
iPSC-Mφ ($2.5–4 \times 10^6$) were transplanted into the lungs of each mouse as described previously (Happle et al., 2014).

CT Scan and Quantification of Lung Opacity

Micro-chest CT images were acquired on a small-animal scanner (eXplore CT120, TriFoil Imaging) in spontaneously breathing, continuously warmed animals anesthetized with 1.0%–1.5% isoflurane. For maximal inspiration and expiration gating, respiratory monitoring was performed. CT acquisition parameters were set to 80 kV, 50 mA, 16-ms exposure time, 386 views, and 0.5° increment angle. For reconstruction, filtered back-projection with a binning of 2 was performed, resulting in isotropic voxel dimensions of 98.3 mm. Post-processing of the in- and expiratory micro-CT datasets was performed on a workstation using the software Visage 7.1.7 (Visage Imaging, Pro Medicus) by two radiologists who were blinded with regard to animal groups as well as in- and expiratory phase imaging. Separate manual segmentation of the right and left lung was performed on representative images, and an interpolation algorithm was applied for the interleaved images. The result was manually refined, assessing the lung contours in the axial, coronal, and sagittal planes. Consensus reading of the segmentation volumes was obtained and, based on these final segmentation volumes, the following data were obtained separately for left and right lung: volume (cm^3), mean density, SD maximum density, and minimum density (all Hounsfield units). The mean density of the whole lung was calculated.

Organs Preparation

BALF was collected from the right lung by flushing 3× with 400 μL PBS. Organs for flow cytometry, as well as genomic DNA isolation, were homogenized through a 150-μm mesh filter (right lung, bone marrow, spleen, liver, and lymph nodes). Left lungs were either cryopreserved or fixed in formalin for immunofluorescence or histology, respectively, and the other organs (liver, spleen, sternum, brain, fat, muscle, kidney, and heart) were fixed in formalin for histology.

Flow Cytometry and FACS

Cells derived from the different organs were blocked with Fc Block (eBioscience) for 20 min at 4°C and then stained with the CD45.1 APC antibody (eBioscience, 17–0453), and or Siglec-F PE antibody (BD Pharmingen, 552126) for 45–60 min at 4°C. CD45.1$^+$ cells of lungs and BALF where then sorted by FACS.

PCR on Genomic DNA

Genomic DNA was isolated from the different organs using the GenElute Mammalian Genomic DNA Miniprep Kit according to the manufacturer's instructions. Purified genomic DNA (200 ng) was used to perform a specific PCR on the 3′ LTR of the integrated reprogramming cassette present in the iPSCs using previously described primers (1 and 3 [Kuehle et al., 2014]), (annealing temperature: 69°C, 40 cycles). Positive internal control PCR utilizing primers described from genotyping of mice (Jackson Laboratory) (annealing temperature: 63°C, 28 cycles).

Clonogenic Assay

A total of 1,500 primary bone marrow-derived lineage-negative cells, and 25,000 or 50,000 iPSC-Mφ, were seeded in a methylcellulose medium (HSC007, R&D Systems) and allowed to grow for 7 days before colonies containing more than 50 cells were counted.

Cytospins

Cells (500–50,000) were spun onto a glass and stained using May-Gruenwald/GIEMSA.

ELISA

The concentration of surfactant protein D (SP-D) and cytokines (GM-CSF and M-CSF) in BALF was measured by ELISA as described (Suzuki et al., 2014b).

Total Protein Concentration

Protein concentrations were measured using a Pierce BCA Protein Assay Kit (Thermo Fischer Scientific) according to the manufacturer's instructions.

Periodic Acid-Schiff Staining

Cryopreserved lungs were completely cut in sequential slides (4 μm). Systematic uniform random sampling was applied to randomly select slides to quantify PAS-positive material (total of 8–10 slides per lung). Periodic acid-Schiff (PAS) staining was performed, following the provider's protocol, with a PAS staining kit (Merck) and hematoxylin (Sigma-Aldrich) as nuclear counterstaining. Slides were automatically scanned with an AxioScanZ.1 (Carl Zeiss), and random subsampling (10% fraction) at 20× magnification was automatically done with NewCAST system software (Visiopharm A/S). Subsampled images were quantified by superimposing a test system (point grid) using the stereological tool Stepanizer (Tschanz et al., 2011), and PAS-positive material was quantified as a fraction of total lung tissue by point counting.

Immunofluorescence

Slides from cryopreserved lungs were fixed and permeabilized for 10 min in 100% ice-cold methanol. Following rehydration in PBS (10 min at room temperature [RT]), blocking was performed with 10% swine serum (Dako, Glostrup, Denmark) in PBS for 30 min. Incubation with antibodies anti-mouse CD68 PE-Cyanine7 (1:200) (eBioscience, 25–0681) and anti-mouse CD45.1 APC (1:200) (eBioscience, 17–0453) was performed for 2 hr at RT. Nuclear counterstaining with DAPI (1:10,000) (Molecular Probes), and pictures were taken with a fluorescence microscope Leica DM6000B (Leica Microsystems).

Histology

Tissues were fixed in 4% paraformaldehyde for at least 24 hr, dehydrated (Shandon Hypercenter XP), and subsequently embedded in paraffin (TES, Medite). Bones were decalcified (0.4 M EDTA [pH 7.2], 4°C for 4–5 days) prior to paraffin embedding. Sections (2–3 μm thick, Reichert-Jung 2030 Microtom) were deparaffinized in xylene and H&E stained according to standard protocols. Blinded evaluation (Axioskop 40 microscope, Zeiss) was performed by a trained pathologist and representative microphotographs were taken (AxioCam MRc, Zeiss).

Statistics

Values for statistical significance have been calculated using GraphPad Prism. The respective method used is given in the figures legends.

REFERENCES

Ackermann, M., Lachmann, N., Hartung, S., Eggenschwiler, R., Pfaff, N., Happle, C., Mucci, A., Gohring, G., Niemann, H., Hansen, G., et al. (2014). Promoter and lineage independent anti-silencing activity of the A2 ubiquitous chromatin opening element for optimized human pluripotent stem cell-based gene therapy. Biomaterials 35, 1531–1542.

Bain, C.C., and Mowat, A.M. (2014). The monocyte-macrophage axis in the intestine. Cell Immunol. 291, 41–48.

Biffi, A., Aubourg, P., and Cartier, N. (2011). Gene therapy for leukodystrophies. Hum. Mol. Genet. 20, R42–R53.

Bleriot, C., Dupuis, T., Jouvion, G., Eberl, G., Disson, O., and Lecuit, M. (2015). Liver-resident macrophage necroptosis orchestrates type 1 microbicidal inflammation and type-2-mediated tissue repair during bacterial infection. Immunity 42, 145–158.

Buchrieser, J., James, W., and Moore, M.D. (2017). Human induced pluripotent stem cell-derived macrophages share ontogeny with MYB-independent tissue-resident macrophages. Stem Cell Reports 8, 334–345.

Cartier, N., Lewis, C.A., Zhang, R., and Rossi, F.M. (2014). The role of microglia in human disease: therapeutic tool or target? Acta Neuropathol. 128, 363–380.

Epelman, S., Lavine, K.J., and Randolph, G.J. (2014). Origin and functions of tissue macrophages. Immunity 41, 21–35.

Gomez Perdiguero, E., Klapproth, K., Schulz, C., Busch, K., Azzoni, E., Crozet, L., Garner, H., Trouillet, C., de Bruijn, M.F., Geissmann, F., et al. (2015). Tissue-resident macrophages originate from yolk-sac-derived erythro-myeloid progenitors. Nature 518, 547–551.

Guilliams, M., De Kleer, I., Henri, S., Post, S., Vanhoutte, L., De Prijck, S., Deswarte, K., Malissen, B., Hammad, H., and Lambrecht, B.N. (2013). Alveolar macrophages develop from fetal monocytes that differentiate into long-lived cells in the first week of life via GM-CSF. J. Exp. Med. 210, 1977–1992.

Happle, C., Lachmann, N., Skuljec, J., Wetzke, M., Ackermann, M., Brennig, S., Mucci, A., Jirmo, A.C., Groos, S., Mirenska, A., et al. (2014). Pulmonary transplantation of macrophage progenitors as effective and long-lasting therapy for hereditary pulmonary alveolar proteinosis. Sci. Transl. Med. 6, 250ra113.

Happle, C., Lachmann, N., Ackermann, M., Mirenska, A., Gohring, G., Thomay, K., Mucci, A., Hetzel, M., Glomb, T., Suzuki, T., et al. (2018). Pulmonary transplantation of human iPSC-derived macrophages ameliorates pulmonary alveolar proteinosis. Am. J. Respir. Crit. Care Med. https://doi.org/10.1164/rccm.201708-1562OC.

Hoeffel, G., Chen, J., Lavin, Y., Low, D., Almeida, F.F., See, P., Beaudin, A.E., Lum, J., Low, I., Forsberg, E.C., et al. (2015). C-Myb(+) erythro-myeloid progenitor-derived fetal monocytes give rise to adult tissue-resident macrophages. Immunity 42, 665–678.

Hussell, T., and Bell, T.J. (2014). Alveolar macrophages: plasticity in a tissue-specific context. Nat. Rev. Immunol. 14, 81–93.

Kleff, V., Sorg, U.R., Bury, C., Suzuki, T., Rattmann, I., Jerabek-Willemsen, M., Poremba, C., Flasshove, M., Opalka, B., Trapnell, B., et al. (2008). Gene therapy of beta(c)-deficient pulmonary alveolar proteinosis (beta(c)-PAP): studies in a murine in vivo model. Mol. Ther. 16, 757–764.

Kolde, R. (2015). pheatmap: Pretty Heatmaps. R package 1.0.8. https://cran.r-project.org/web/packages/pheatmap/index.html.

Kovtunovych, G., Ghosh, M.C., Ollivierre, W., Weitzel, R.P., Eckhaus, M.A., Tisdale, J.F., Yachie, A., and Rouault, T.A. (2014). Wild-type macrophages reverse disease in heme oxygenase 1-deficient mice. Blood 124, 1522–1530.

Kuehle, J., Turan, S., Cantz, T., Hoffmann, D., Suerth, J.D., Maetzig, T., Zychlinski, D., Klein, C., Steinemann, D., Baum, C., et al. (2014). Modified lentiviral LTRs allow Flp recombinase-mediated cassette exchange and in vivo tracing of "factor-free" induced pluripotent stem cells. Mol. Ther. 22, 919–928.

Lachmann, N., Happle, C., Ackermann, M., Luttge, D., Wetzke, M., Merkert, S., Hetzel, M., Kensah, G., Jara-Avaca, M., Mucci, A., et al. (2014). Gene correction of human induced pluripotent stem cells repairs the cellular phenotype in pulmonary alveolar proteinosis. Am. J. Respir. Crit. Care Med. *189*, 167–182.

Lachmann, N., Ackermann, M., Frenzel, E., Liebhaber, S., Brennig, S., Happle, C., Hoffmann, D., Klimenkova, O., Luttge, D., Buchegger, T., et al. (2015). Large-scale hematopoietic differentiation of human induced pluripotent stem cells provides granulocytes or macrophages for cell replacement therapies. Stem Cell Reports *4*, 282–296.

Ladner, M.B., Martin, G.A., Noble, J.A., Wittman, V.P., Warren, M.K., McGrogan, M., and Stanley, E.R. (1988). cDNA cloning and expression of murine macrophage colony-stimulating factor from L929 cells. Proc. Natl. Acad. Sci. USA *85*, 6706–6710.

Lavin, Y., Winter, D., Blecher-Gonen, R., David, E., Keren-Shaul, H., Merad, M., Jung, S., and Amit, I. (2014). Tissue-resident macrophage enhancer landscapes are shaped by the local microenvironment. Cell *159*, 1312–1326.

Litvack, M.L., Wigle, T.J., Lee, J., Wang, J., Ackerley, C., Grunebaum, E., and Post, M. (2016). Alveolar-like stem cell-derived Myb(-) macrophages promote recovery and survival in airway disease. Am. J. Respir. Crit. Care Med. *193*, 1219–1229.

Martinez-Moczygemba, M., Doan, M.L., Elidemir, O., Fan, L.L., Cheung, S.W., Lei, J.T., Moore, J.P., Tavana, G., Lewis, L.R., Zhu, Y., et al. (2008). Pulmonary alveolar proteinosis caused by deletion of the GM-CSFRalpha gene in the X chromosome pseudoautosomal region 1. J. Exp. Med. *205*, 2711–2716.

Mucci, A., Kunkiel, J., Suzuki, T., Brennig, S., Glage, S., Kuhnel, M.P., Ackermann, M., Happle, C., Kuhn, A., Schambach, A., et al. (2016). Murine iPSC-derived macrophages as a tool for disease modeling of hereditary pulmonary alveolar proteinosis due to Csf2rb deficiency. Stem Cell Reports *7*, 292–305.

Naldini, L. (2015). Gene therapy returns to centre stage. Nature *526*, 351–360.

Neri, T., Muggeo, S., Paulis, M., Caldana, M.E., Crisafulli, L., Strina, D., Focarelli, M.L., Faggioli, F., Recordati, C., Scaramuzza, S., et al. (2015). Targeted gene correction in osteopetrotic-induced pluripotent stem cells for the generation of functional osteoclasts. Stem Cell Reports *5*, 558–568.

Nishinakamura, R., Nakayama, N., Hirabayashi, Y., Inoue, T., Aud, D., McNeil, T., Azuma, S., Yoshida, S., Toyoda, Y., Arai, K., et al. (1995). Mice deficient for the IL-3/GM-CSF/IL-5 beta c receptor exhibit lung pathology and impaired immune response, while beta IL3 receptor-deficient mice are normal. Immunity *2*, 211–222.

Pfaff, N., Lachmann, N., Kohlscheen, S., Sgodda, M., Arauzo-Bravo, M.J., Greber, B., Kues, W., Glage, S., Baum, C., Niemann, H., et al. (2012). Efficient hematopoietic redifferentiation of induced pluripotent stem cells derived from primitive murine bone marrow cells. Stem Cells Dev. *21*, 689–701.

Sgambato, J.A., Park, T.S., Miller, D., Panicker, L.M., Sidransky, E., Lun, Y., Awad, O., Bentzen, S.M., Zambidis, E.T., and Feldman, R.A. (2015). Gaucher disease-induced pluripotent stem cells display decreased erythroid potential and aberrant myelopoiesis. Stem Cells Transl. Med. *4*, 878–886.

Soucie, E.L., Weng, Z., Geirsdottir, L., Molawi, K., Maurizio, J., Fenouil, R., Mossadegh-Keller, N., Gimenez, G., VanHille, L., Beniazza, M., et al. (2016). Lineage-specific enhancers activate self-renewal genes in macrophages and embryonic stem cells. Science *351*, aad5510.

Sugimura, R., Jha, D.K., Han, A., Soria-Valles, C., da Rocha, E.L., Lu, Y.F., Goettel, J.A., Serrao, E., Rowe, R.G., Malleshaiah, M., et al. (2017). Haematopoietic stem and progenitor cells from human pluripotent stem cells. Nature *545*, 432–438.

Suzuki, N., Yamazaki, S., Yamaguchi, T., Okabe, M., Masaki, H., Takaki, S., Otsu, M., and Nakauchi, H. (2013). Generation of engraftable hematopoietic stem cells from induced pluripotent stem cells by way of teratoma formation. Mol. Ther. *21*, 1424–1431.

Suzuki, T., Arumugam, P., Sakagami, T., Lachmann, N., Chalk, C., Sallese, A., Abe, S., Trapnell, C., Carey, B., Moritz, T., et al. (2014a). Pulmonary macrophage transplantation therapy. Nature *514*, 450–454.

Suzuki, T., Maranda, B., Sakagami, T., Catellier, P., Couture, C.Y., Carey, B.C., Chalk, C., and Trapnell, B.C. (2011). Hereditary pulmonary alveolar proteinosis caused by recessive CSF2RB mutations. Eur. Respir. J. *37*, 201–204.

Suzuki, T., Mayhew, C., Sallese, A., Chalk, C., Carey, B.C., Malik, P., Wood, R.E., and Trapnell, B.C. (2014b). Use of induced pluripotent stem cells to recapitulate pulmonary alveolar proteinosis pathogenesis. Am. J. Respir. Crit. Care Med. *189*, 183–193.

Takahashi, K., and Yamanaka, S. (2006). Induction of pluripotent stem cells from mouse embryonic and adult fibroblast cultures by defined factors. Cell *126*, 663–676.

Takata, K., Kozaki, T., Lee, C.Z.W., Thion, M.S., Otsuka, M., Lim, S., Utami, K.H., Fidan, K., Park, D.S., Malleret, B., et al. (2017). Induced-pluripotent-stem-cell-derived primitive macrophages provide a platform for modeling tissue-resident macrophage differentiation and function. Immunity *47*, 183–198.e6.

Tanaka, T., Motoi, N., Tsuchihashi, Y., Tazawa, R., Kaneko, C., Nei, T., Yamamoto, T., Hayashi, T., Tagawa, T., Nagayasu, T., et al. (2011). Adult-onset hereditary pulmonary alveolar proteinosis caused by a single-base deletion in CSF2RB. J. Med. Genet. *48*, 205–209.

Trapnell, C., Roberts, A., Goff, L., Pertea, G., Kim, D., Kelley, D.R., Pimentel, H., Salzberg, S.L., Rinn, J.L., and Pachter, L. (2012). Differential gene and transcript expression analysis of RNA-seq experiments with TopHat and Cufflinks. Nat. Protoc. *7*, 562–578.

Trapnell, C., Williams, B.A., Pertea, G., Mortazavi, A., Kwan, G., van Baren, M.J., Salzberg, S.L., Wold, B.J., and Pachter, L. (2010). Transcript assembly and quantification by RNA-Seq reveals unannotated transcripts and isoform switching during cell differentiation. Nat. Biotechnol. *28*, 511–515.

Tschanz, S.A., Burri, P.H., and Weibel, E.R. (2011). A simple tool for stereological assessment of digital images: the STEPanizer. J. Microsc. *243*, 47–59.

Tyanova, S., Temu, T., Sinitcyn, P., Carlson, A., Hein, M.Y., Geiger, T., Mann, M., and Cox, J. (2016). The Perseus computational platform for comprehensive analysis of (prote)omics data. Nat. Methods *13*, 731–740.

van Wilgenburg, B., Browne, C., Vowles, J., and Cowley, S.A. (2013). Efficient, long term production of monocyte-derived macrophages from human pluripotent stem cells under partly-defined and fully-defined conditions. PLoS One *8*, e71098.

Varemo, L., Nielsen, J., and Nookaew, I. (2013). Enriching the gene set analysis of genome-wide data by incorporating directionality of gene expression and combining statistical hypotheses and methods. Nucleic Acids Res. *41*, 4378–4391.

Viana, G.M., Buri, M.V., Paredes-Gamero, E.J., Martins, A.M., and D'Almeida, V. (2016). Impaired hematopoiesis and disrupted monocyte/macrophage homeostasis in mucopolysaccharidosis type I mice. J. Cell Physiol. *231*, 698–707.

Xu, P., Tong, Y., Liu, X.Z., Wang, T.T., Cheng, L., Wang, B.Y., Lv, X., Huang, Y., and Liu, D.P. (2015). Both TALENs and CRISPR/Cas9 directly target the HBB IVS2-654 (C > T) mutation in beta-thalassemia-derived iPSCs. Sci. Rep. *5*, 12065.